

A multiscale framework for the origin and variability of the South Pacific Convergence Zone

Adrian J. Matthews*

School of Environmental Sciences and School of Mathematics, University of East Anglia, Norwich, UK

*Correspondence to: A. J. Matthews, School of Environmental Sciences, University of East Anglia, Norwich Research Park, Norwich, NR4 7TJ, UK. E-mail: a.j.matthews@uea.ac.uk

The diagonal South Pacific Convergence Zone (SPCZ) is the major climatological precipitation feature over the Pacific region during the Northern Hemisphere winter. However, the basic mechanisms that control its structure and variability are only partly understood. Here, an analysis of the SPCZ is carried out in a multiscale framework. This identifies two modes that dominate: a (westward) shifted SPCZ and an enhanced SPCZ, which occur independently of each other. Within both modes, the primary mechanism for the initiation of precipitation is a transient synoptic wave propagating along the subtropical jet, which is then refracted by the basic state toward the westerly duct over the central equatorial Pacific. Individual vorticity centres in the wave become elongated, with a diagonal (northwest–southeast) tilt. Convection then occurs in a diagonal band in the poleward flow ahead of the cyclonic vorticity anomaly in the wave. However, latent heat release in the convection leads to upper-tropospheric divergence and anticyclonic vorticity forcing, which dissipates the wave, shutting off the convective forcing and stopping the precipitation. Hence, each individual wave or event only lasts a few days and contributes a discrete pulse of diagonally oriented precipitation to the region. The sum of these events leads to the diagonal climatological SPCZ. Event occurrence is a stochastic process, the probability of which is modified by lower-frequency variability of the basic state, including the Madden–Julian Oscillation (MJO) and El Niño–Southern Oscillation (ENSO). For example, during periods of enhanced convection over the eastern Indian Ocean to western Pacific (MJO phases 3–6 and La Niña) the westerly duct expands westwards, allowing synoptic waves to refract equatorwards earlier and increasing the probability of westward-shifted SPCZ events. Hence, both the existence and variability of the SPCZ depend fundamentally on scale interactions between dynamical processes on time-scales ranging from daily to interannual. Copyright © 2012 Royal Meteorological Society

Key Words: tropical–extratropical interaction; MJO; ENSO; El Niño; La Niña; SPCZ

Received 4 October 2011; Revised 21 November 2011; Accepted 28 November 2011; Published online in Wiley Online Library

Citation: Matthews AJ. 2012. A multiscale framework for the origin and variability of the South Pacific Convergence Zone. *Q. J. R. Meteorol. Soc.* DOI:10.1002/qj.1870

1. Introduction

The tropical warm pool of high sea-surface temperature (SST; Figure 1(b)) over the Indian Ocean–maritime

continent–western Pacific supports the Earth’s most extensive region of deep convection and heavy precipitation. This extends eastward over the Pacific: *zonally* in the Northern Hemisphere to form the intertropical convergence zone

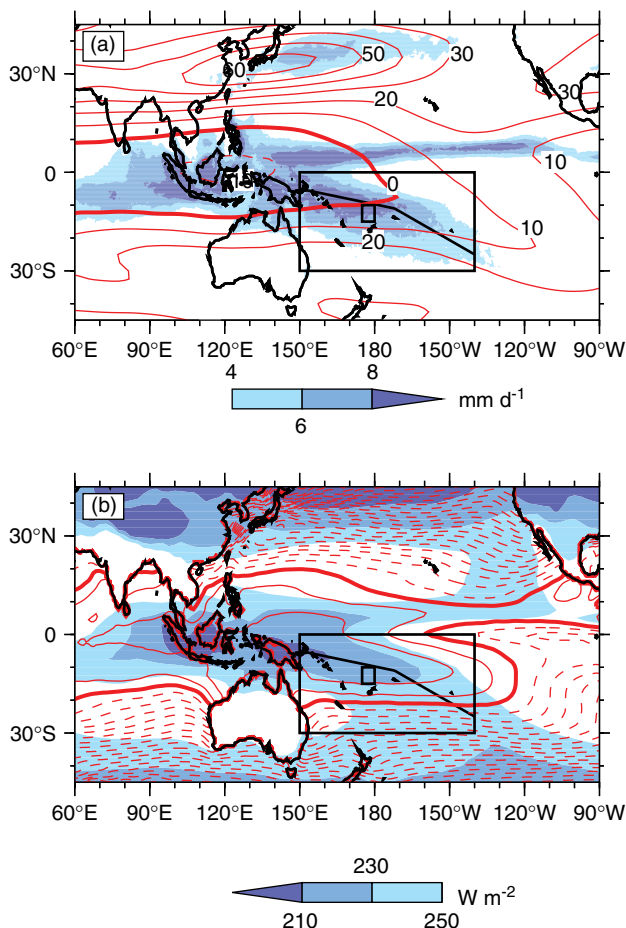


Figure 1. Time-mean (November–April) of (a) TRMM precipitation rate, 200 hPa zonal wind and (b) OLR, SST. Boxes show the domain of EOF analysis and the area of the power spectra. The thick jointed line shows the axis of the SPCZ (maximum precipitation). The shading interval for TRMM precipitation rate is 2 mm d^{-1} (see legend). The contour interval for the 200 hPa zonal wind is 10 m s^{-1} ; the zero contour is thick and negative contours are dotted. The shading interval for OLR is 20 W m^{-2} (see legend). The contour interval for SST is $1 \text{ }^{\circ}\text{C}$; the $27 \text{ }^{\circ}\text{C}$ contour is thick and contours below $27 \text{ }^{\circ}\text{C}$ are dotted. This figure is available in colour online at wileyonlinelibrary.com/journal/qj

(ITCZ) along 8°N and *diagonally* in the Southern Hemisphere to form the South Pacific Convergence Zone (SPCZ; Figure 1(a)).

The SPCZ (Vincent, 1994) supplies rainfall locally for the communities on the southwest Pacific islands. Precipitation on these islands has significant variability on many time-scales: the Madden–Julian Oscillation (MJO) on intraseasonal time-scales (Matthews and Li, 2005); the El Niño–Southern Oscillation (ENSO) on interannual time-scales and the Interdecadal Pacific Oscillation (IPO: Folland *et al.*, 2002) and longer time-scales (Griffiths *et al.*, 2003). The SPCZ environment itself provides the necessary conditions for, and is the main location of, tropical cyclogenesis in the South Pacific (Vincent *et al.*, 2011). The SPCZ precipitation is also important globally. Due to its large spatial scale and strength, the latent heat release in the SPCZ rivals that over the maritime continent, at the heart of the warm pool. This latent heating leads to a significant dynamical response through the excitation of Rossby waves that will impact on global climate.

It was recognized early on that during northern winter tropical–extratropical interaction is important for triggering convection along both the diagonal SPCZ (Streten, 1973)

and the zonal ITCZ (Kiladis and Weickmann, 1992a). During northern summer, these interactions are much reduced and the SPCZ itself is much weaker. The basic reason is the presence of the ‘westerly duct’ (Webster and Holton, 1982) over the equatorial Pacific during northern winter. At this time, the highest sea-surface temperatures (SSTs) and precipitation in the warm pool to the west are centred on the Equator (Figure 1). The equatorial Kelvin-wave response to the associated latent heating (Gill, 1980) leads to upper tropospheric westerly flow on the Equator to the east, over the Pacific (Figure 1(a)). This is reinforced by equatorward advection of westerly momentum from the subtropical jets by flow around the upper tropospheric anticyclone pair that flanks the equatorial heating, as part of the equatorial Rossby-wave response (Jin and Hoskins, 1995). The westerly duct in the upper troposphere along with the easterly trade winds in the lower troposphere make up the Walker cell.

During northern summer, the warm-pool precipitation moves northward off the Equator. The latent heating then projects less favourably on the equatorial Kelvin-wave structure and the westerly duct gives way to mean easterly winds over the Pacific that extend through the whole depth of the troposphere.

The existence, or not, of the westerly duct changes the propagation characteristics of transient Rossby waves, which are the main agents of the tropical–extratropical interaction in the SPCZ and ITCZ. Hoskins and Ambrizzi (1993) considered the propagation of barotropic Rossby waves in a realistic mean upper tropospheric flow, using ray-tracing and Wentzel–Kramers–Brillouin (WKB) theory. Stationary Rossby waves can propagate freely in regions of mean westerlies but are evanescent in regions of mean easterlies, with the dividing zero-wind line acting as a critical line. Furthermore, the spatial distribution of the mean westerly winds (e.g. jet locations and strengths) acts to refract the Rossby waves. The subtropical westerly jets act as waveguides, channelling Rossby waves along them. The westerlies over the equatorial Pacific during northern winter allow cross-equatorial propagation of Rossby waves from one hemisphere to another, hence a westerly ‘duct’. This is in contrast to northern summer, when mean easterly winds extend all the way around the Equator, forming a barrier between the two hemispheres. Further refinements, allowing for the baroclinic component of the waves (Ambrizzi and Hoskins, 1997) and relaxing the stationary assumption (i.e. allowing for non-zero phase speed: Yang and Hoskins, 1996) did not qualitatively change the main results.

The propagation of Rossby waves in a spatially varying mean flow can also be interpreted in terms of accumulation of wave energy (Webster and Holton, 1982). In particular, in jet-exit regions where the mean westerly wind \bar{u} decreases eastward ($\partial\bar{u}/\partial x < 0$), the zonal wavenumber will increase along a ray path. This leads to a decrease in the wave group speed and an increase in the wave energy density (Webster and Chang, 1998). When applied in the region of the SPCZ (Widlansky *et al.*, 2011), this can explain the observation that the SPCZ acts as a synoptic ‘graveyard’ (Trenberth, 1976).

Once these transient waves have propagated over the SPCZ and ITCZ regions, their internal structure can trigger convection there. Consistent with quasi-geostrophic theory, the waves have ascent and reduced static stability in the poleward flow ahead of their cyclonic vorticity anomalies or

upper-tropospheric pressure troughs (Hoskins *et al.*, 1985). In the Tropics, in regions susceptible to deep convection (high SST, conditionally unstable atmosphere), this forcing from the transient waves can trigger deep convection and precipitation. Observed transient convection over the ITCZ in northern winter has been explained by this mechanism (Kiladis and Weickmann, 1992a,b, 1997; Kiladis, 1998). General circulation models are also able to replicate this sequence of events (Slingo, 1998).

Lower frequency variability of these processes in the ITCZ has been observed to be due to variations in the basic state and subsequent propagation of Rossby waves during the MJO (Matthews and Kiladis, 1999a) and ENSO (Matthews and Kiladis, 1999b). When there was active convection over the maritime continent during either the MJO or ENSO (La Niña), then there was a strong westerly duct over the equatorial eastern Pacific and a weak subtropical jet over the North Pacific. These changes to the basic state acted on Rossby waves propagating out of the Asian jet and enhanced their equatorward refraction into the westerly duct. This led to an enhancement of transient convection over the ITCZ, which rectified back onto the lower frequency modulation, producing enhanced convection throughout the active maritime-continent phase of the MJO and throughout a La Niña event. Conversely, when there was suppressed convection over the maritime continent and enhanced convection over the western Pacific, during the MJO or ENSO (El Niño), the opposite was observed; the westerly duct was weak and waves tended to propagate zonally along the strengthened North Pacific jet waveguide. Hence there was less transient convection over the ITCZ, which rectified into a suppressed convection anomaly there during that phase of the MJO and ENSO. These observational results were confirmed by barotropic model and ray-tracing experiments under these different basic states (Matthews and Kiladis, 2000).

The triggering of transient convection by equatorward-propagating wave trains also appears to be at work over the SPCZ (Kiladis and Weickmann, 1992a). These processes are also modified by ENSO on interannual time-scales (Widlansky *et al.*, 2011).

An alternative mechanism for SPCZ convection involves a direct forcing from the maritime continent (Matthews *et al.*, 1996). Here, equatorial convection associated with the MJO forces an equatorial Rossby-wave response with an anticyclone pair in the upper troposphere. The southern hemisphere anticyclone interacts with the subtropical jet over Australia, advecting large-magnitude (negative, cyclonic) potential vorticity (PV) equatorwards on its eastern flank. This cyclonic PV anomaly then induces ascent and convection on its eastern side (over the SPCZ region), in a similar manner to the convection induced by the cyclonic anomalies in the transient wave trains.

Although the proximate cause of the precipitation in the SPCZ appears to be the convection triggered in the transient wave trains, the background basic state in which the wave trains and convection develop is also of paramount importance. Ultimately, this basic state and in particular the difference between the diagonal SPCZ in the Southern Hemisphere and the zonal ITCZ in the Northern Hemisphere must be due to the asymmetries in the global distribution of ocean, land and orography.

For example, the topographic barrier of the Andes induces a planetary-wave response with subsidence and a subtropical

anticyclone over the eastern Pacific (Takahashi and Battisti, 2007). Air with low moist static energy is advected around this dry zone near the surface, maintaining a distinct diagonal alignment to the northeast edge of the SPCZ. Transient variability in the trade winds can also impact on this dry zone and the location of the eastern edge of the SPCZ (Lintner and Neelin, 2008). The effect of the Andes on the SPCZ may also be transmitted indirectly through its control of the SST, as when the Andes were removed in an atmospheric general circulation model (GCM) experiment but the observed SST distribution was retained, the SPCZ was still successfully simulated (Kiladis *et al.*, 1989).

Despite the importance of the diagonal SPCZ to tropical rainfall and global climate, its underlying dynamics and physical mechanisms are not fully understood, as they depend on a complex mixture of tropical and extratropical atmospheric dynamics and interaction with the ocean. This is reflected in a systematic error common to most climate models, that the simulated SPCZ has too zonal an orientation (Brown *et al.*, 2011). Some key questions concerning the SPCZ still remain.

- (1) The transient waves that trigger the SPCZ convection have been interpreted in a dry adiabatic framework. What is the role of the substantial diabatic heating in the wave-induced SPCZ convection on the waves themselves?
- (2) What is the exact nature of the variability of the SPCZ, in particular the interactions between transient waves that are the proximate cause of convection over the SPCZ and the major lower-frequency modes of variability in the region, the MJO and ENSO?
- (3) Why is the SPCZ diagonal and the ITCZ zonal, particularly as precipitation in both is triggered by equatorward-propagating transient waves?

Following the conceptual framework put forward by Meehl *et al.* (2001), lower frequency climate variations are assumed to set the basic state on which higher frequency variability develops. The aggregated effects of the modified higher frequency variability then feed back on to the lower frequency variations and climatology. In this article, we examine the SPCZ using global observational datasets in a multiscale framework to assess the mechanisms and interplays behind it. This allows us to put forward physical mechanisms for both the origin and variability of the SPCZ based on scale interactions between different dynamical components of the Pacific region.

2. Data

The interpolated outgoing long-wave radiation (OLR) dataset of Liebmann and Smith (1996) was used as a proxy for tropical convection. The data used were daily means on a $2.5^\circ \times 2.5^\circ$ grid from 1979–2009. These were supplemented by the Tropical Rainfall Measuring Mission (TRMM) merged precipitation (3B42) dataset (Kummerow *et al.*, 2000) from 1998–2009. The data were on a $0.25^\circ \times 0.25^\circ$ grid at 3 h resolution. Low values of OLR (Figure 1(b)) correspond to high values of precipitation (Figure 1(a)) in the Tropics, and negative OLR anomalies correspond to positive precipitation anomalies.

Dynamical fields (horizontal wind, vertical velocity, sea-level pressure) were taken as daily means on a $2.5^\circ \times 2.5^\circ$

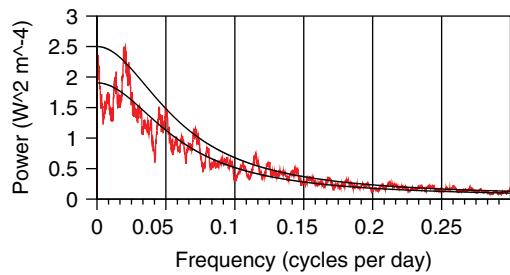


Figure 2. The 31 point smoothed power spectrum of daily OLR averaged over the box from 175–180°E, 10–15°S (see Figure 1). A red-noise background spectrum and its 95% confidence limit are shown by the thick lines. This figure is available in colour online at wileyonlinelibrary.com/journal/qj

grid from the National Center for Environmental Prediction–Department of the Environment (NCEP–DOE) reanalysis (Kanamitsu *et al.*, 2002). Data were extracted for the same period as the OLR data: 1979–2009. SST data were extracted from the NOAA Optimum Interpolation (OI v2) dataset (Reynolds *et al.*, 2002) for the period 1982–2009. These were on a $1^\circ \times 1^\circ$ grid as weekly means, which were then interpolated to daily means for ease of analysis.

An annual cycle (mean plus first three [five for precipitation] annual harmonics) was calculated for each variable then subtracted to produce daily anomaly fields.

3. Primary modes of SPCZ variability

3.1. Multiple time-scales

For a preliminary examination of the variability within the SPCZ, a time series was constructed by area-averaging the daily anomalous OLR over a box in the heart of the SPCZ (175–180°E, 10–15°S; small box in Figure 1). The power spectrum of this time series was then calculated and smoothed by a $L = 31$ point running mean (Figure 2). A theoretical background red-noise spectrum was calculated (lower thick line in Figure 2), assuming that the time series was generated by a first-order Markov process and using the lag-1 autocorrelation coefficient of 0.69 calculated from the time series (Wilks, 2005). The 95% confidence interval (upper thick line in Figure 2) was calculated by a chi-squared test using $2L$ degrees of freedom.

There is a large peak at the lowest, interannual frequencies. There are then significant peaks in an intraseasonal band centred at a frequency of $0.025 \text{ cycle day}^{-1}$ (cpd; 40 d period) and in the submonthly band (frequency 0.075 cpd ; 13 d period). These spectral peaks are consistent with the SPCZ variability associated with ENSO, MJO and Rossby-wave activity, respectively, as discussed in section 1. Hence, later analysis was carried out in three frequency bands to assess the multiscale interactions in the SPCZ. Lanczos filters (Duchon, 1979) were used to isolate the three frequency bands: a 200 d low-pass filter for interannual variability, a 20–200 d bandpass filter for intraseasonal variability and a 20 d high-pass filter for submonthly variability.

However, first an objective analysis of SPCZ variability was performed on unfiltered daily data to isolate the dominant modes of variability across all time-scales. To do this, an empirical orthogonal function (EOF) analysis (Wilks, 2005) was carried out on daily OLR anomalies over the wider SPCZ domain (150°E–140°W, 0–30°S). This domain covers

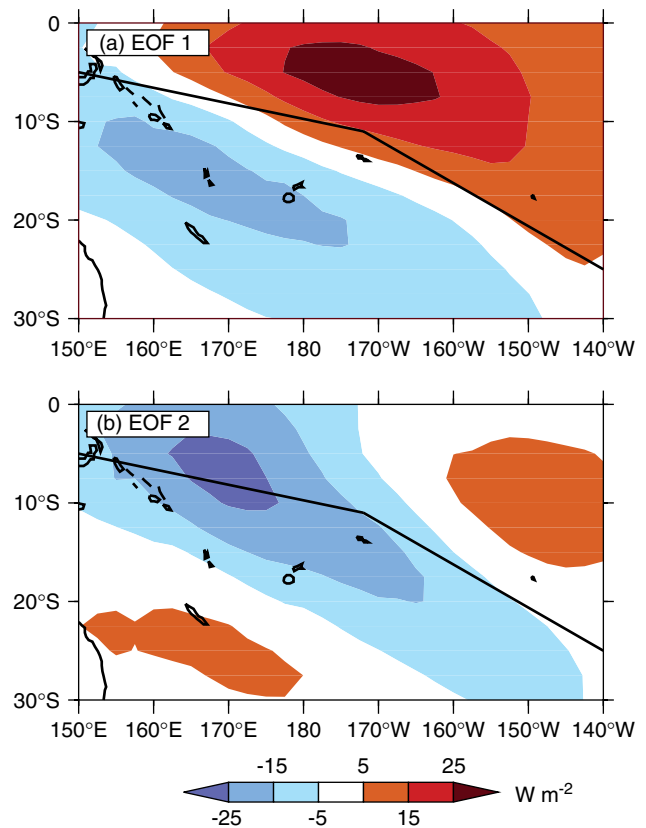


Figure 3. The leading EOFs of daily unfiltered OLR over the SPCZ domain (150°E–140°W, 0–30°S) for northern winter. (a) EOF 1, (b) EOF 2. The shading interval for OLR anomalies is 10 W m^{-2} (see legend). The SPCZ axis is shown by the jointed line, as in Figure 1. (c) Time series of PC 1 (solid line) and PC 2 (dotted line) for the sample winter of 2001–2002. This figure is available in colour online at wileyonlinelibrary.com/journal/qj

both the subtropical and diagonal portions of the SPCZ (large box in Figure 1). Only data from northern winter (November–April) were used, as this is the time of year when the SPCZ is most active. The OLR dataset was used in preference to the TRMM precipitation, due to its longer length (31 yr compared with 12 yr).

Two clear modes of SPCZ variability arise from the EOF analysis. EOF 1 accounts for 12.0% of the variance and describes an SPCZ that is shifted southwestward (Figure 3(a)). Negative OLR anomalies (enhanced convection) lie to the southwest of the position of the mean SPCZ axis and positive OLR anomalies (reduced convection) are to the northeast. EOF 2 (8.8% of the variance) describes an enhancement of the tropical part of the SPCZ, but with a more horizontally tilted diagonal part with reduced convection either side (Figure 3(b)). These two leading

EOFs are well separated from each other and from the higher EOFs (which form a degenerate set), according to the criteria of North *et al.* (1982).

The principal component (PC) time series (daily amplitude of the spatial EOF patterns) are shown for a typical winter (2001–2002, Figure 3(c)). Both time series show variability over a wide range of time-scales, consistent with the broad-band variability of the OLR spectrum from the heart of the SPCZ (Figure 2). There is no clear phase relationship between variations in PC 1 and PC 2. Hence the modes of variability appear to be uncorrelated.

3.2. Shifted SPCZ mode

The shifted SPCZ mode of EOF 1 can be viewed as a natural perturbation experiment. By diagnosing the mechanisms by which the SPCZ moves, specific insights into its fundamental origins may be gained. This is potentially more productive than examining mean SPCZ conditions (or just a straightforward enhancement of the mean), as in this situation it is more difficult to evaluate which processes are relevant to the SPCZ and which are not.

An event-compositing approach was used to diagnose the shifted SPCZ mode further. An event was defined when two criteria were satisfied: an amplitude criterion that PC 1 was above a threshold of +1 standard deviation and a relative criterion that PC 1 was a maximum compared with all its neighbours out to five days before and after the event. The relative criterion was necessary so that each coherent event was only counted once, five days being a suitable time interval between the synoptic waves that will be shown to be behind this SPCZ mode.

Over the 30 winters analyzed, there were 171 events (approximately one per month). The event occurrence followed a clear seasonal cycle, with a maximum occurring in January (37 events) when the northern-winter basic state is at its strongest. At the beginning and end of the extended winter season, only 26 and 24 events occurred in November and April respectively. For information only, event occurrence was also calculated for the northern summer months. It decreased considerably, with only 6 events in July. These northern summer months were *not* included in the subsequent analysis. Hence, using the 171 northern winter events only, composites were constructed as the mean of a particular field over these 171 days. Statistical significance was established by a Student *t*-test. Lagged composites were similarly constructed.

By design, the day-zero (zero lag) composite of the unfiltered OLR anomaly shows a southwest-shifted SPCZ (Figure 4(c)), with a northwest–southeast oriented band of negative OLR anomalies in the southwestern part of the SPCZ domain and positive OLR anomalies to the northeast. The southwest-shifted SPCZ is also linked to enhanced convection (negative OLR anomalies) over the equatorial maritime continent.

Transient convection in the diagonal SPCZ is known to be triggered by equatorward-propagating waves in the upper troposphere (e.g. Kiladis and Weickmann, 1992a). Consistent with previous studies, the associated dynamical structure here shows a wave train in the 200 hPa vorticity anomalies. The northwest–southeast aligned band of convection in the shifted SPCZ is to the east (ahead) of a similarly aligned negative vorticity anomaly or cyclone (labelled C1 in Figure 4(c)). The enhanced SPCZ convection

is in the region of southeastward flow (significant 200 hPa wind-vector anomalies) ahead of this cyclone. This poleward flow will ascend up the sloping mean isentropes. Hence, the shifted SPCZ convection is consistent with that triggered in a baroclinic wave or midlatitude cyclone in the quasi-geostrophic framework. Similar results were obtained by Kiladis and Weickmann (1992b), but the square boxes they used to area-average the OLR and regress on to did not capture the diagonal tilt in the SPCZ convection and circulation anomalies obtained using the EOF analysis in this study.

Moving further downstream, ahead of cyclone C1, there is a northwest–southeast oriented anticyclone (A1). The significant northwestward flow ahead of this anticyclone flows down the sloping mean isentropes, providing the stabilizing conditions for the suppressed convection in this region. However, although the strongest suppressed convection (positive OLR anomalies above $15W^{-2}$) is elongated and oriented northwest–southeast, there is also weakly suppressed convection extending further east into the central equatorial Pacific. Further northeast there is another negative (cyclonic) vorticity anomaly C2 that is also tilted northwest–southeast. This cyclonic anomaly is in the deep Tropics (centred at $10^{\circ}S$, $150^{\circ}W$).

These three vorticity anomalies (C1, A1, C2) are part of an even larger wave train that extends back along the subtropical jet over the Indian Ocean and Australia along approximately $40^{\circ}S$ and then curves northeastward over the SPCZ region, shown by the thick curved line in Figure 4(c).

The orientation of the wave train and its propagation is consistent with that in a dry barotropic model linearized about a 300 hPa northern-winter mean flow (Hoskins and Ambrizzi, 1993, their figure 10). In both the observations here and the model, a fairly circular vorticity anomaly upstream in the jet leads into a northwest–southeast elongated anomaly propagating northeastward over the Australian–western Pacific domain. Hence, the elongation of the wave train can be qualitatively explained by dry Rossby-wave dynamics propagating on the mean state. This wave-train orientation appears to be the first step in explaining the diagonal orientation of the SPCZ.

The temporal evolution of the wave train and convection can be tracked using the other (lagged) composites in Figure 4. At day -6 there is no enhanced convection in the SPCZ region (Figure 4(a)). The wave train is located further upstream, to the west. Cyclone C1 is over southeastern Australia, while anticyclone A1 extends eastwards from the Coral Sea. There is already enhanced convection over the maritime continent, with associated 200 hPa anomalous easterly flow over the tropical Indian Ocean. At the eastern edge of the SPCZ domain the suppressed convection is also already present, along with cyclone C2.

At day -3 (Figure 4(b)), the enhanced convection over the maritime continent and the easterly anomalies over the Indian Ocean persist, as do the suppressed convection and cyclone C2 in the eastern SPCZ domain. The wave train along the subtropical jet has developed and propagated eastward. Enhanced convection is now developing at the tropical end of the shifted SPCZ, over the Coral Sea.

By day 0 (Figure 4(c)) the wave train is fully developed, along with the enhanced convection along the shifted SPCZ. The suppressed convection over the central tropical Pacific expands westwards, as it is reinforced by the descending southeasterly winds ahead of anticyclone A1. By day 3

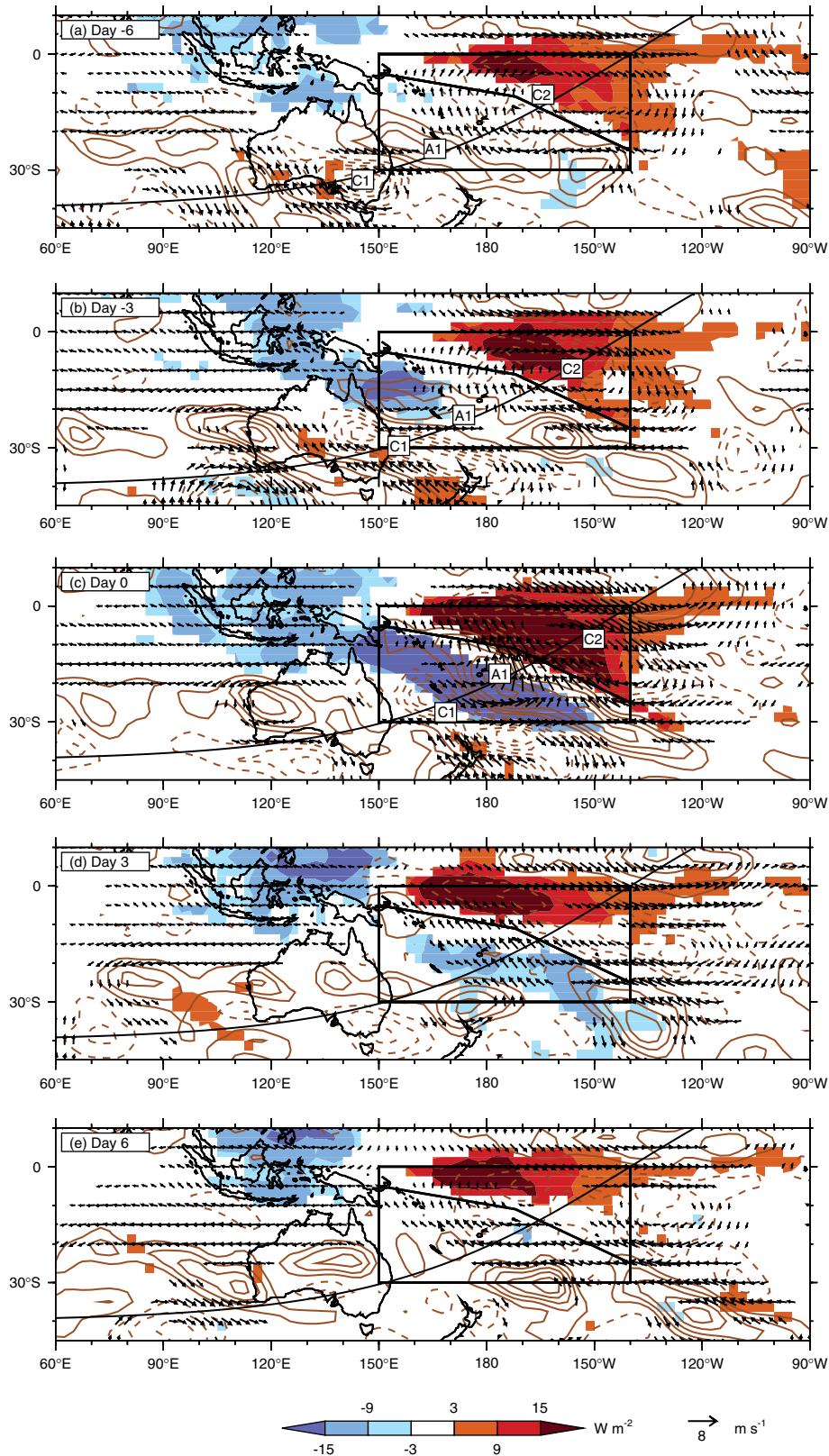


Figure 4. Lagged composites of unfiltered OLR and 200 hPa vorticity and vector wind anomalies on days (a) -6 , (b) -3 , (c) 0 , (d) 3 and (e) 6 , for the shifted SPCZ mode (EOF 1). The shading interval for OLR anomalies is 6 W m^{-2} (see legend). The contour interval for the 200 hPa vorticity anomaly is $2 \times 10^{-6} \text{ s}^{-1}$; negative contours are dashed and the zero contour is omitted. The reference vector for the 200 hPa vector wind anomalies has magnitude 8 m s^{-1} . The vorticity and vector wind anomalies are only plotted where they are significant at the 95% level. The box shows the SPCZ region from the EOF analysis. The SPCZ axis is shown by the jointed line. The curved line indicates the path of wave propagation. This figure is available in colour online at wileyonlinelibrary.com/journal/qj

(Figure 4(d)) the suppressed convection has moved further westward and become confined to the Equator. The wave train has lost coherence (especially cyclone C1) and the enhanced shifted SPCZ convection is also weakening. However, the enhanced maritime-continent convection is still active. By day 6 (Figure 4(e)) the diagonal SPCZ convective anomalies have all disappeared. However, we are still left with the enhanced convection over the maritime continent, which has been slowly moving eastward since day -6, and the suppressed convection near the dateline.

From this complex sequence of events, several distinct phenomena can be extracted, acting on different time-scales.

- (1) The southwest-shifted SPCZ appears to be forced by the equatorward incursion of a midlatitude transient wave train, with the enhanced convection in the ascending poleward flow ahead of a cyclonic anomaly, consistent with Kiladis and Weickmann (1992a). The diagonal orientation of the wave train and subsequent SPCZ convection appears to be due to the propagation and dispersion of the wave train on the mean state, consistent with the model experiments of Hoskins and Ambrizzi (1993) in a dry dynamical framework.
- (2) Enhanced convection over the maritime continent is present throughout the whole period and the transient convection in the shifted diagonal SPCZ appears to be anchored to this, suggesting a role for the MJO or ENSO.
- (3) There is also a long-lived suppressed convective anomaly that propagates slowly westward from the central equatorial Pacific into the SPCZ region. This has a large-scale upper tropospheric cyclonic anomaly associated with it and is consistent with a convectively coupled equatorial Rossby-wave structure (Wheeler and Kiladis, 1999). The poleward flank of this suppressed convection is then reinforced by the descending flow ahead of the anticyclone in the transient wave train, leading to a diagonal structure.

These phenomena are investigated further by separating the analysis into different frequency bands, as described in section 3.1.

3.2.1. Submonthly contribution: tropical incursion of an extratropical wave train

Lagged composite maps of 20 d high-pass filtered data were constructed to examine the submonthly contributions to the SPCZ variability (Figure 5). They clearly isolate the role of the equatorward incursion of the midlatitude wave train. On day -4 (Figure 5(a)) the wave train is propagating along the jet at 35°S and has already begun its equatorward incursion. Cyclone C1, over eastern Australia, is elongated and has a weak northwest-southeast tilt. At this stage there is no enhanced convection ahead of it. Further downstream, anticyclone A1 actually has suppressed convection ahead of it, over the SPCZ region, on these fast time-scales.

By day -2 (Figure 5(b)) the wave has propagated downstream such that cyclone C1 is now over the SPCZ region, with some weakly enhanced convection ahead of it over the Coral Sea. On day 0 (Figure 5(c)) the wave train and the convective anomalies along the diagonal SPCZ are at maximum amplitude. However, by day 2 (Figure 5(d)) both the wave train and the SPCZ convective anomalies

have rapidly died away. Note that there are no convective or wind anomalies over the maritime continent or equatorial Pacific in the submonthly patterns, as these are of lower frequency. Hence the basic convection along the diagonal SPCZ is governed by the high-frequency waves.

The dynamical origin of the transient wave train is examined through a vertical section along its curved propagation path (Figure 6(a)). The vorticity anomalies are maximum in the upper troposphere at 200 hPa. They show a pronounced tilt with height towards the left, i.e. westwards or southwestwards, against the propagation direction. This is consistent with the wave train growing through baroclinic conversion on a mean flow with westerly vertical shear. The vertical extent H of the circulation that such upper-level (potential) vorticity anomalies induce is given by the Prandtl-Rossby-Burger relation $H \sim fL/N$, where f is the Coriolis parameter, L is the horizontal length-scale and N is the buoyancy frequency (e.g. Hoskins *et al.*, 1985). In the extratropical portion of the section, $|f|$ is large and the circulation anomalies extend down to near the surface. In the tropical part of the section, $|f|$ is small and the induced flow is restricted to the upper troposphere.

The temporal behaviour of the wave train and its associated convection is shown in a Hovmöller diagram along the propagation path (Figure 6(b)). The downstream phase propagation of the vorticity anomalies (e.g. the negative vorticity anomaly of cyclone C1) can be clearly seen along the upstream part of the section. As the cyclone propagates equatorward into the SPCZ region it generates enhanced convection (a negative OLR anomaly) ahead of it, which peaks on day 0 (Figure 6(b), cf. Figures 4(c) and 5(c)). The subsequent rapid disruption and decay of the wave train and convection after day 0 can clearly be seen in Figure 6(b). In particular, there is no indication that the convective anomalies propagate; they grow and decay *in situ*.

As the disruption and decay of the wave train only happens after its embedded SPCZ convection has been triggered, the convection may have a direct role in this demise. In particular, the latent heat release associated with the convection is substantial; 20 day high-pass-filtered precipitation anomalies are over $r = 4 \text{ mm d}^{-1}$, corresponding to a latent heat release of $Q = L\rho_w r = 120 \text{ W m}^{-2}$, where $L = 2.5 \times 10^6 \text{ J kg}^{-1}$ is the latent heat of vaporization of water and $\rho_w = 1000 \text{ kg m}^{-3}$ is the density of water. This diabatic heating enhances the ascent in the wave, leading to increased divergence in the upper troposphere. This divergent outflow is an anticyclonic vorticity source and will counter the cyclonic vorticity tendency as the cyclone C1 propagates over the region of convection. A scale analysis reveals the strength of this effect. The 200 hPa divergence anomaly associated with the SPCZ convection has an amplitude of $D \sim 4 \times 10^{-6} \text{ s}^{-1}$ (Figure 7). The anticyclonic vorticity tendency from the vortex-stretching term is $\partial\xi/\partial t = -fD \sim 2 \times 10^{-5} \text{ s}^{-1} \text{ d}^{-1}$, using a value for the Coriolis parameter of $f = -5 \times 10^{-5} \text{ s}^{-1}$ at 20°S. The magnitude of the cyclonic anomaly C1 at this time is $\xi' \sim -1 \times 10^{-5} \text{ s}^{-1}$ (Figure 7). Hence the vortex-stretching tendency is strong enough to remove this in less than a day, consistent with the rapid decay of the wave train from this time (Figure 5(c) and (d)). Upstream in the wave, and at earlier times, the divergence anomaly is much smaller. Hence, the destruction of the wave train appears to be due

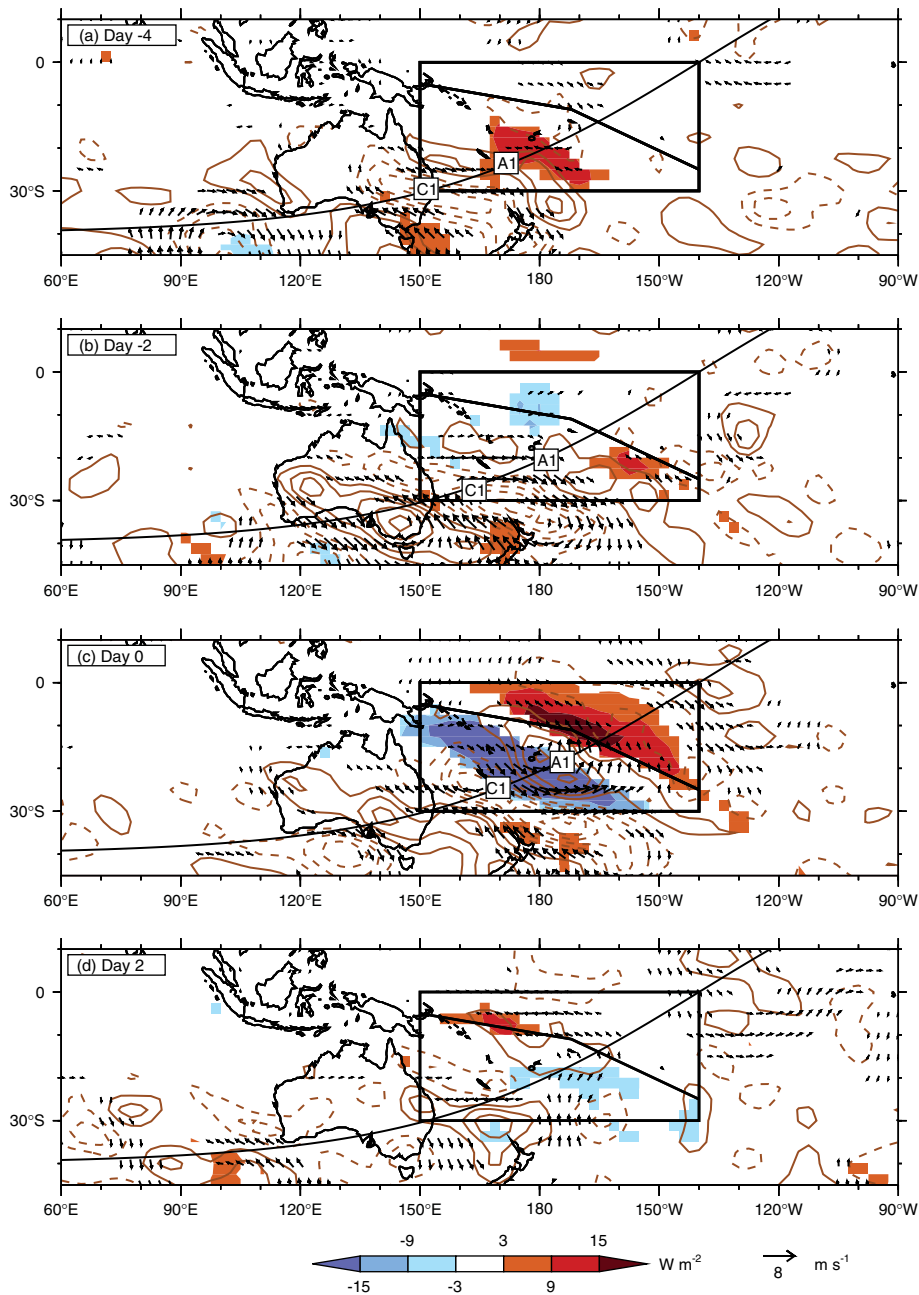


Figure 5. As for Figure 4, but for 20 day high-pass filtered data, on day (a) -4 , (b) -2 , (c) 0 and (d) 2 . This figure is available in colour online at wileyonlinelibrary.com/journal/qj

to the diabatic heating and is not just part of the adiabatic wave dynamics.

3.2.2. Intraseasonal contribution: MJO and equatorial Rossby wave









The generation of convection along the shifted SPCZ appears to be controlled by the equatorward incursion of the high-frequency (20 day high-pass filtered) wave trains, as discussed in section 3.2.1. Now we investigate the modulation of these processes by lower-frequency variations in the climate system, starting with the intraseasonal band.

At day -8 , the 20–200 day filtered composite shows enhanced convection (negative OLR anomalies) and upper-tropospheric easterly wind anomalies over the equatorial Indian Ocean (Figure 8(a)). By day 0 , when the enhanced convection peaks over the SPCZ (by design), the equatorial

convection has propagated eastward to the maritime continent (Figure 8(b)). The upper-tropospheric vorticity and wind anomalies in the subtropics are relatively weak on these intraseasonal time-scales (note the difference in the standard wind vectors between Figures 5 and 8) and there is no obvious wave-train structure. However, the slow eastward propagation of the equatorial convective anomalies is indicative of the MJO.

The modulation of the shifted SPCZ events by the MJO is shown in Table 1. First, the unconditional probability of a shifted SPCZ event occurring on a randomly chosen day is calculated as $\hat{p} = n/N = 3.1\%$, where $n = 171$ is the total number of shifted SPCZ events and $N = 5438$ is the total number of days in the study period. The daily occurrence probabilities of a shifted SPCZ event are then calculated for each phase of the MJO, as defined by the Wheeler and Hendon (2004) index. When no MJO is present the daily

Table 1. Modulation of SPCZ event occurrence by the MJO. The number of days and number of SPCZ events in each MJO phase are N and n , respectively. If the probability \hat{p} of the daily occurrence of an SPCZ event is significant at the 95% level, it is shown in bold if enhanced and italics if suppressed. The thumbnails indicate the regions of enhanced convection (blue in the online article) and reduced convection (red in the online article) during each MJO phase.

	Shifted SPCZ			Enhanced SPCZ	
	N	n	$\hat{p}(\%)$	n	$\hat{p}(\%)$
All days	5438	171	3.1	198	3.6
No MJO	1968	64	3.2	62	3.1
MJO Phase 1 	345	2	0.6	14	4.1
MJO Phase 2 	428	13	3.0	7	1.6
MJO Phase 3 	497	19	3.8	12	2.4
MJO Phase 4 	439	19	4.3	12	2.7
MJO Phase 5 	404	22	5.4	19	4.7
MJO Phase 6 	456	17	3.7	28	6.1
MJO Phase 7 	491	9	1.8	33	6.7
MJO Phase 8 	410	6	1.5	11	2.7

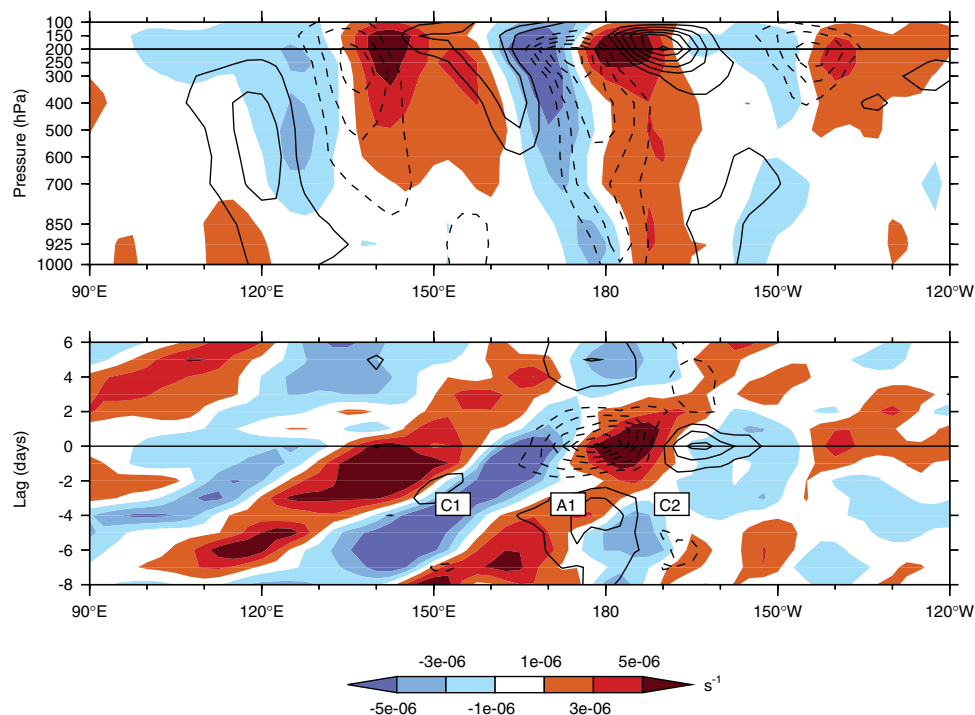


Figure 6. Composites of 20 day high-pass filtered data for the shifted SPCZ mode (EOF 1) in sections along the curved propagation path (curved line in e.g. Figure 5(c)). (a) Vertical section of vorticity (shaded) and meridional wind (line contour) anomalies at zero lag. (b) Hovmöller diagram of 200 hPa vorticity (shaded) and OLR (line contour) anomalies. The shading interval for the vorticity is $2 \times 10^{-6} \text{ s}^{-1}$ (see legend). Contour intervals are 0.5 m s^{-1} for the meridional wind and 5 W m^{-2} for OLR; negative contours are dashed and the zero contour is omitted. This figure is available in colour online at wileyonlinelibrary.com/journal/qj

probability of a shifted SPCZ event (3.2%) is not significantly different from the unconditional value. However, when an MJO is present the daily probability of a shifted SPCZ event is significantly enhanced during MJO phases 3–6 and significantly reduced during MJO phases 7–8–1. Statistical significance is calculated as in Hall *et al.* (2001).

Note (from the thumbnails in Table 1) that changes to the frequency of SPCZ events are not necessarily reflected in the convective anomalies for the MJO phases. For example, during MJO phase 3 there is a strongly enhanced frequency of SPCZ events but the slowly varying envelope of MJO convection is only enhanced over the eastern Indian Ocean. Hence it appears that it is the slowly varying MJO changes to the basic state in which the high-frequency waves are

developing that cause the changes to the SPCZ, rather than a direct low-frequency change.

The basic state along the Equator is characterized by upper-tropospheric mean easterlies over the maritime continent and western Pacific and the westerly duct over the central and eastern Pacific, separated by the zero-wind line. The changes to this basic state between MJO phases 3–6 (when there are significantly more shifted SPCZ events) and MJO phases 7–8–1 (when the shifted SPCZ events are relatively infrequent) are shown in Figure 9. During MJO phases 3–6, the zero-wind line (thick solid contour in Figure 9) crosses the Equator at 178°E , compared with 158°W in MJO phases 7–8–1 (thick dotted contour in Figure 9). Hence, the westerly duct has expanded westwards, allowing

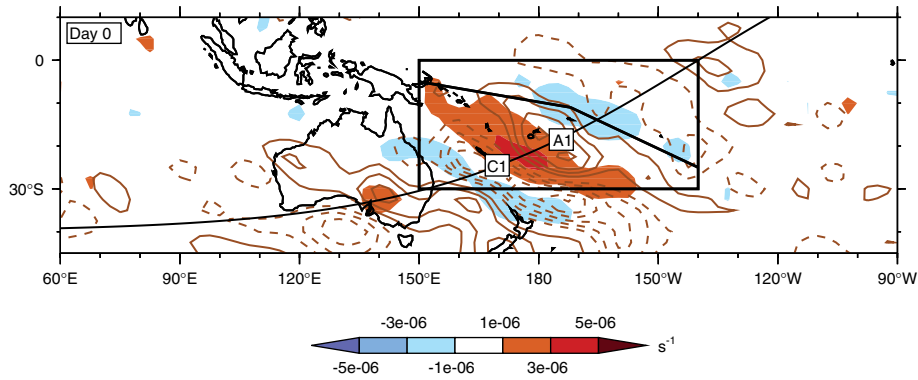


Figure 7. Zero-lagged composites of 20 day high-pass filtered 200 hPa divergence and vorticity anomalies for the shifted SPCZ mode (EOF 1). The shading interval for the divergence is $2 \times 10^{-6} \text{ s}^{-1}$ (see legend). The contour interval for the vorticity is $2 \times 10^{-6} \text{ s}^{-1}$; negative contours are dashed and the zero contour is omitted. This figure is available in colour online at wileyonlinelibrary.com/journal/qj

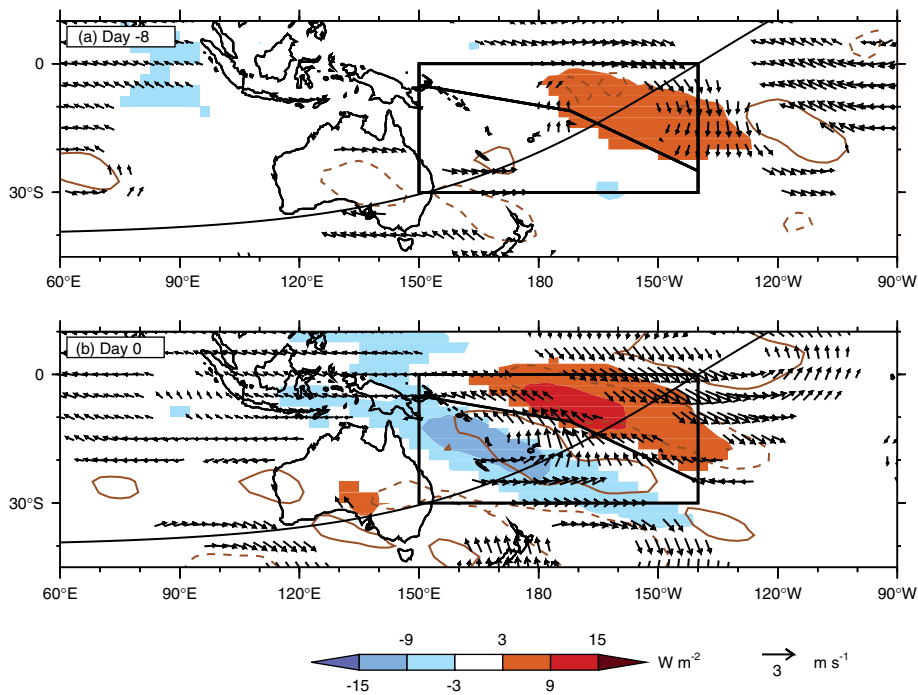


Figure 8. As Figure 4 but for 20–200 day filtered data on days (a) –8 and (b) 0. The standard vector for the 200 hPa wind has magnitude 3 m s^{-1} . This figure is available in colour online at wileyonlinelibrary.com/journal/qj

synoptic waves to begin their equatorward propagation further west than usual, leading to the shifted SPCZ. This equatorward propagation of the transient waves will also be aided by the equatorward MJO flow over Australia (5 m s^{-1} southerlies, in Figure 9).

As well as influencing the propagation characteristics of the transient waves, the MJO changes to the basic state also have an effect on the convection and precipitation within those waves. During phases 3–6, the MJO equatorial convection is active from the Indian Ocean through to the maritime continent (thumbnails in Table 1). This is reflected in the negative 500 hPa omega anomalies in the region (Figure 9), indicating MJO ascent. The large-scale response to the convective latent heating then also includes subtropical ascent over the shifted SPCZ region (southwest corner of the box in Figure 9), further aiding the precipitation in the transient waves. To the northeast, over the mean SPCZ position, there is descent from the MJO, suppressing any convection in the transient waves.

3.2.3. Interannual contribution: ENSO

The influence of interannual variability, particularly ENSO, on the shifted SPCZ mode is now examined. The composite of 200 day low-pass filtered OLR for the shifted SPCZ events shows a convective dipole along the Equator, with enhanced convection over the maritime continent and reduced convection over the central Pacific (Figure 10). By design, there are also negative OLR anomalies along the shifted SPCZ. The large-scale upper-tropospheric winds are consistent with an equatorial Rossby-wave response to the equatorial convective forcing, with an anticyclone flanking the enhanced convection and a cyclone flanking the reduced convection. The composite is at zero lag but, given the 200 day low-pass filter used here, composites within lags of $\pm 30 \text{ d}$ are very similar. Hence, the basic state is effectively constant on these time-scales throughout the lifetime of any individual shifted SPCZ event.

Such a low-frequency convective dipole is reminiscent of La Niña. The number and frequency of daily occurrence of

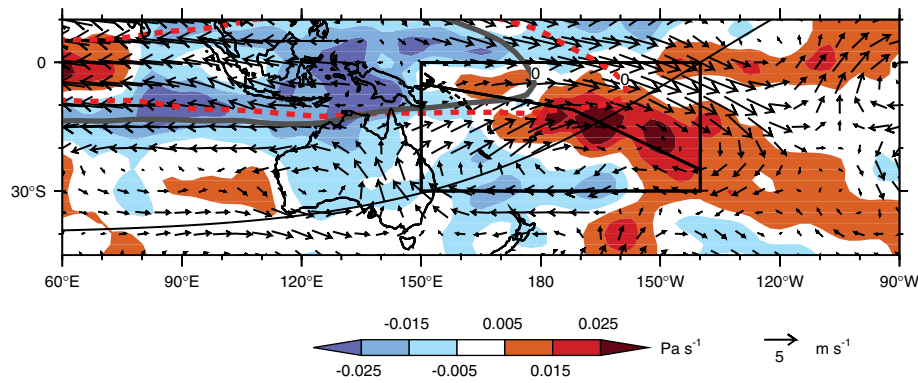


Figure 9. Change in basic state of 500 hPa vertical velocity (ω) and 200 hPa vector wind during the MJO (mean during MJO phases 3–6 minus the mean during MJO phases 7–8–1). The shading interval for ω is 0.01 Pa s^{-1} (see legend). The standard wind vector has magnitude 5 m s^{-1} . A thick contour shows the zero mean zonal wind line (dividing westerlies from easterlies) during MJO phases 3–6 (solid) and MJO phases 7–8–1 (dotted). This figure is available in colour online at wileyonlinelibrary.com/journal/qj

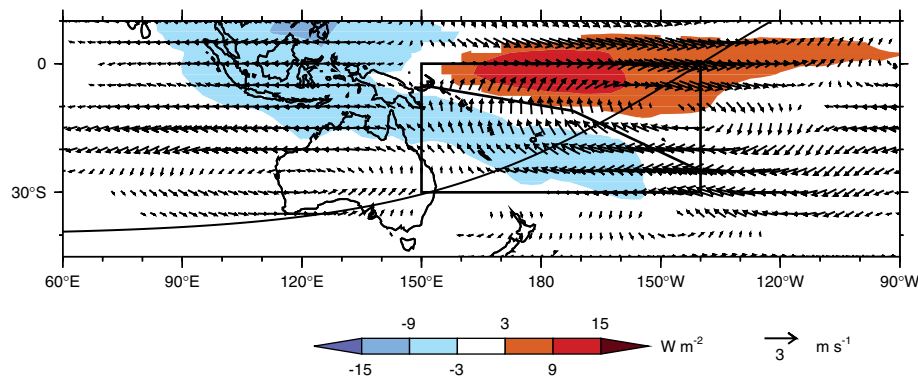


Figure 10. As Figure 4 but for 200 day low-pass filtered data on day 0. The standard vector for the 200 hPa wind has magnitude 3 m s^{-1} . This figure is available in colour online at wileyonlinelibrary.com/journal/qj

Table 2. As Table 1, but for modulation by ENSO.

	Shifted SPCZ			Enhanced SPCZ	
	N	n	$\hat{p}(\%)$	n	$\hat{p}(\%)$
All	5438	171	3.1	198	3.6
ENSO Neutral	3712	126	3.4	147	4.0
El Niño	1001	4	0.4	30	3.0
La Niña	725	41	5.7	21	2.9

shifted SPCZ events during El Niño and La Niña periods are shown in Table 2. El Niño is defined as the situation when the NINO3.4 index is above 1, La Niña when it is below -1 . As with the MJO analysis in section 3.2.2, the frequency of daily occurrence of a shifted SPCZ event is $\hat{p} = 3.1\%$. This is not significantly changed during ENSO-neutral periods ($\hat{p} = 3.4\%$). However, during El Niño periods the frequency is significantly reduced (only $n = 4$ events, giving a daily occurrence of $\hat{p} = 0.4\%$). During La Niña periods there is a significant increase in the occurrence of shifted SPCZ events ($n = 41$, $\hat{p} = 5.7\%$).

This modulation of the shifted SPCZ event occurrence by ENSO can be explained by a change in the basic state, similar to the modulation by the MJO discussed in section 3.2.2. The zero mean wind line is shown in Figure 11 for La Niña (thick solid line) and El Niño (thick dotted line). The westerly duct expands westwards

during La Niña, allowing the extratropical waves to refract equatorward further westwards, leading to the shifted SPCZ. Equally prominently, there are positive SST anomalies to the southwest of the mean SPCZ axis and negative SST anomalies to the northeast (Figure 11), providing a thermodynamic forcing of the convection in the shifted SPCZ events.

Although certain phases of low-frequency variability (active MJO over eastern Indian Ocean and maritime continent; La Niña) do significantly modulate the frequency of occurrence of shifted SPCZ events, they are not necessary conditions for the shifted SPCZ events to occur. For example, 37% of the SPCZ events happened when no MJO was present, and (an overlapping) 74% of SPCZ events were in ENSO-neutral conditions. Hence the SPCZ events can be viewed as a stochastic process, with the changes to the basic state provided by the MJO and ENSO changing the probability distribution of the events.

3.3. Enhanced SPCZ mode

Analysis of the shifted SPCZ mode (EOF 1; Figure 3(a)) has led to insights into the mechanisms governing the variability of the SPCZ. This approach was particularly fruitful because EOF 1 represented a distinct change from the normal SPCZ. Hence conditions that led to the shifted SPCZ were themselves different from normal and therefore easier to identify.

We now turn to EOF 2 (Figure 3(b)): the ‘enhanced’ SPCZ mode. This mode essentially represents the activity of the SPCZ in its climatological position, although it does

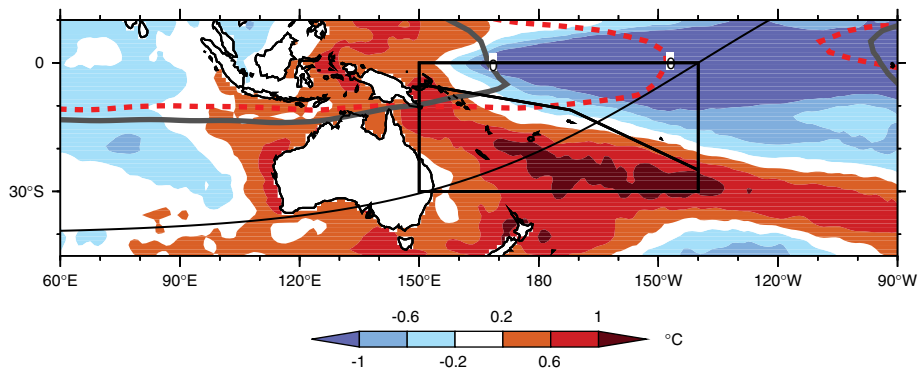


Figure 11. Change in the basic state of SST during ENSO (La Niña minus El Niño). The shading interval for SST is $0.4\text{ }^{\circ}\text{C}$ (see legend). A thick contour shows the zero mean zonal wind line (dividing westerlies from easterlies) during La Niña (solid) and El Niño (dotted). This figure is available in colour online at wileyonlinelibrary.com/journal/qj

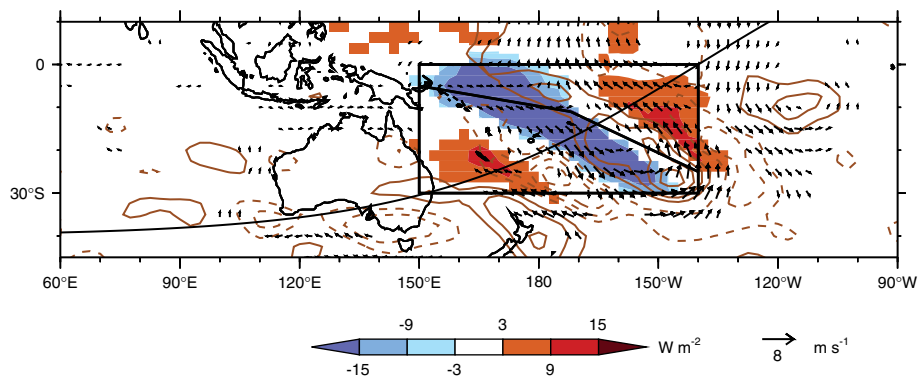


Figure 12. As for Figure 5, but for the enhanced SPCZ mode (EOF 2) on day 0. This figure is available in colour online at wileyonlinelibrary.com/journal/qj

have a steeper northwest–southeast tilt than the climatology. Only a brief description of this mode is given, as it offers similar insights to those gained from the shifted SPCZ mode.

The basic mechanism behind the enhanced SPCZ mode is the same as that for the shifted SPCZ mode. A total of $n = 198$ enhanced SPCZ events were identified. Composites of unfiltered (not shown) and 20 day high-pass filtered (Figure 12) anomalies confirm that the enhanced SPCZ mode is also triggered by the equatorward incursion of an extratropical synoptic wave train into the westerly duct. However, rather than occurring to the west of the climatological SPCZ as in the shifted mode, the incursion of the wave train and the triggering of the diagonal convection lie approximately along the line of the climatological SPCZ. As with the shifted SPCZ mode, diagonal convection in the enhanced SPCZ mode appears to grow and decay *in situ*, with no propagation once it has developed.

The enhanced SPCZ mode is also modulated by the lower frequency variability. It occurs preferentially during MJO phases 5–7 and is suppressed during MJO phases 8, 2–4 (Table 1), i.e. at a later and further eastward stage of the MJO than the shifted SPCZ mode. Although there are no significant interannual (200 day low-pass filtered) SST anomalies associated with the enhanced SPCZ mode, the mode is modulated by ENSO. It has a significantly reduced frequency of occurrence during *both* El Niño and La Niña (Table 2). This can be explained by the enhanced SPCZ mode being an expression of mean SPCZ conditions; both El Niño and La Niña basic states are different from the climatology and will not favour this mode.

4. Discussion and conclusions

A multiscale analysis of the SPCZ during northern winter has been carried out to assess the mechanisms behind its origin and variability. Two modes of variability were found: a shifted SPCZ mode and an enhanced SPCZ mode. The fundamental mechanism behind the occurrence of each mode or SPCZ event is the equatorward incursion of synoptic wave trains from the Southern Hemisphere subtropical jet into the westerly duct over the central and eastern equatorial Pacific. The refraction of these waves as they propagate on the basic state initially gives rise to their diagonal (northwest–southeast) tilt. Once over the high SSTs of the tropical western Pacific, the ascent ahead of the tilted cyclone in the wave triggers a similar diagonally tilted band of convection and precipitation.

The diabatic heating from condensation of water vapour in the convection leads to ascent and upper-level divergence. The anticyclonic vorticity tendency from this divergence is strong enough to spin down the initial cyclonic part of the wave train and effectively dissipate the wave. Hence each individual wave can deliver a pulse of diagonally oriented convection to the SPCZ region. The mean diagonal SPCZ is then the sum of these diagonal pulses or events.

The variability of the SPCZ is due to the exact locations at which these events occur. The occurrence of the events can be viewed as a stochastic process. The probabilities of the event occurring at a given location are then modified by other, lower-frequency variations to the basic state. In particular, the MJO and ENSO modify the SPCZ event probabilities on intraseasonal and interannual time-scales, respectively. When convection is anomalously active between the eastern

Indian Ocean and the western Pacific, during MJO phases 3–6 or a La Niña, the daily probability of a westward-shifted SPCZ event increases significantly (it almost doubles during a La Niña). Conversely, when there is active convection over the central Pacific during MJO phases 7–8–1 or an El Niño, the daily probability of a shifted SPCZ event is significantly reduced (by a factor of 8 during an El Niño). This is at least partly due to the change in the basic state. Active convection over the eastern Indian Ocean to western Pacific leads to a relative retraction of the equatorial upper-tropospheric easterlies over that region and a westward expansion of the westerly duct into the western Pacific. Synoptic waves propagating along the subtropical jet in the Southern Hemisphere are then refracted equatorwards earlier (i.e. further upstream or westward) than usual, such that subsequent triggering of diagonal SPCZ convection is also further westward.

A further intriguing question, raised in the Introduction, is why the SPCZ in the Southern Hemisphere is diagonal while the ITCZ in the Northern Hemisphere is zonal. Given the nature of the diagonal orientation of the wave trains and the diagonal convection they induce, it might be more appropriate to turn the question around. A diagonal band of convection appears to be the default starting position for convection triggered by equatorward refraction and propagation of synoptic waves into the equatorial westerly duct. Why then is the ITCZ zonal? The answer possibly lies in the underlying SST distribution.

In the Southern Hemisphere during northern winter, the high SSTs occupy a broad latitudinal area (Figure 1(b)). Convection can then be triggered along the entire extensive diagonal band ahead of the tilted cyclonic anomaly in a wave train. Hence the SPCZ is diagonal. This configuration is further aided by the diagonal SST gradient and cooler SSTs at the 'back' of the SPCZ (Figure 1(b)), partly due to the existence of the Andes and the strong South Pacific High (Takahashi and Battisti, 2007).

In the Northern Hemisphere a similar mechanism operates. Equatorward refraction of synoptic waves toward the westerly duct also leads to diagonally oriented (southwest–northeast) cyclonic anomalies. However, the underlying SST distribution is latitudinally much more confined, with a zonal maximum along 8°N flanked by lower SSTs to the north and the equatorial cold tongue to the south (Figure 1(b)). The resulting precipitation is then a convolution of the diagonal forcing region sliding across the fixed zonal SST distribution, producing a zonal precipitation region or ITCZ.

Another factor is likely to be the different jet structures and land–sea and topography distributions in the two hemispheres. In the Northern Hemisphere, the subtropical jet is flanked on its equatorward side by the Tibetan Plateau and is strong and narrow over the western Pacific (Figure 1(a)). Hence, it acts like a highly effective waveguide (Hoskins and Ambrizzi, 1993). Waves do not 'leak' out of the waveguide and propagate equatorwards until they are over the central and eastern Pacific (Kiladis and Weickmann, 1992b). Here, over the eastern part of the Pacific basin, they encounter the equatorial cold tongue and zonal SST distribution as discussed above. However, in the Southern Hemisphere there is no equivalent topographic barrier, as Australia is relatively low-lying and the jet structure is broader. This leads to a weaker waveguide, with the result that waves can begin to propagate equatorwards earlier

and then encounter the wider, more homogeneous SST distribution in the western part of the Pacific basin. The internal mechanism of wave dynamics, induced convection and diabatic-heating-induced spin-down then leads to the diagonal orientation of the SPCZ.

The analysis here has focused on the upper tropospheric dynamics, where the main Rossby-wave propagation occurs. However, the extratropical wave trains also have a surface component, with low-pressure synoptic centres and embedded fronts. The concept of the SPCZ as a 'graveyard' of fronts (Trenberth, 1976) can potentially be incorporated into the framework of upper tropospheric wave dynamics presented here. However, the fronts themselves have their own internal dynamics and may also play a more active role in the SPCZ.

The mechanisms proposed here for the diagonal orientation of the SPCZ and the zonal orientation of the ITCZ are inferences from an analysis of observational data. They could be tested by a targeted set of numerical model experiments, which is currently being planned.

These mechanisms are also likely to be relevant to the weaker diagonal convergence zones found in the other ocean basins: the South Atlantic Convergence Zone (SACZ: Pohl *et al.*, 2009; Hart *et al.*, 2010) and the South Indian Convergence Zone (SICZ: Cook, 2000).

Acknowledgements

The interpolated OLR, NCEP Reanalysis and NOAA_OI_SST_V2 data were provided by the NOAA/OAR/ESRL PSD, Boulder, Colorado, USA, from their web site at <http://www.cdc.noaa.gov/>. The TRMM 3B42 data were obtained from NASA-Goddard DAAC, from their website at <http://disc.gsfc.nasa.gov/services/opendap/>. The NINO3.4 index data were obtained from the Climate Prediction Center from their website at <http://www.cpc.ncep.noaa.gov>. The Wheeler and Hendon (2004) MJO index data were obtained from the Centre for Australian Weather and Climate Research from their website at <http://www.cawcr.gov.au/staff/mwheeler/maproom/>.

The research presented in this article was carried out on the High Performance Computing Cluster supported by the Research Computing Service at the University of East Anglia. This work benefited greatly from discussions held at the International Scientific Workshop on the South Pacific Convergence Zone, Apia, Samoa, in August 2010. I thank the Australian Government's Pacific Climate Change Science Program for funding my attendance at the workshop. I thank Ian Renfrew and two anonymous reviewers, whose comments helped to improve the manuscript.

References

- Ambrizzi T, Hoskins BJ. 1997. Stationary Rossby-wave propagation in a baroclinic atmosphere. *Q. J. R. Meteorol. Soc.* **123**: 919–928.
- Brown JR, Power SB, Delage FP, Colman RA, Moise AF, Murphy BF. 2011. Evaluation of the South Pacific Convergence Zone in IPCC AR4 climate model simulations of the twentieth century. *J. Climate* **24**: 1565–1582.
- Cook KH. 2000. The south Indian convergence zone and interannual rainfall variability over southern Africa. *J. Climate* **13**: 3789–3804.
- Duchon CE. 1979. Lanczos filtering in one and two dimensions. *J. Appl. Meteorol.* **18**: 1016–1022.
- Folland CK, Renwick JA, Salinger MJ, Mullan AB. 2002. Relative influences of the Interdecadal Pacific Oscillation and ENSO on the South Pacific Convergence Zone. *Geophys. Res. Lett.* **29**: 1643. DOI:10.1029/2001GL014201.

- Gill AE. 1980. Some simple solutions for heat-induced tropical circulation. *Q. J. R. Meteorol. Soc.* **106**: 447–462.
- Griffiths GM, Salinger MJ, Leleu I. 2003. Trends in extreme daily rainfall across the South Pacific and relationship to the South Pacific Convergence Zone. *Int. J. Climatol.* **23**: 847–869.
- Hall JD, Matthews AJ, Karoly DJ. 2001. The modulation of tropical cyclone activity in the Australian region by the Madden–Julian Oscillation. *Mon. Weather Rev.* **129**: 2970–2982.
- Hart NCG, Reason CJC, Fauchereau N. 2010. Tropical–extratropical interactions over Southern Africa: Three cases of heavy summer season rainfall. *Mon. Weather Rev.* **138**: 2608–2623.
- Hoskins BJ, Ambrizzi T. 1993. Rossby-wave propagation on a realistic longitudinally varying flow. *J. Atmos. Sci.* **50**: 1661–1671.
- Hoskins BJ, McIntyre ME, Robertson AW. 1985. On the use and significance of isentropic potential vorticity maps. *Q. J. R. Meteorol. Soc.* **111**: 877–946.
- Jin F-F, Hoskins BJ. 1995. The direct response to heating in a baroclinic atmosphere. *J. Atmos. Sci.* **52**: 307–319.
- Kanamitsu M, Ebisuzaki W, Woollen J, Yang SK, Hnilo JJ, Fiorino M, Potter GL. 2002. NCEP–DOE AMIP-II Reanalysis (R-2). *Bull. Am. Meteorol. Soc.* **83**: 1631–1643.
- Kiladis GN. 1998. An observational study of Rossby waves linked to convection over the eastern tropical Pacific. *J. Atmos. Sci.* **55**: 321–339.
- Kiladis GN, Weickmann KM. 1992a. Extratropical forcing of tropical Pacific convection during northern winter. *Mon. Weather Rev.* **120**: 1924–1939.
- Kiladis GN, Weickmann KM. 1992b. Circulation anomalies associated with tropical convection during northern winter. *Mon. Weather Rev.* **120**: 1900–1923.
- Kiladis GN, Weickmann KM. 1997. Horizontal structure and seasonality of large-scale circulations associated with submonthly tropical convection. *Mon. Weather Rev.* **125**: 1997–2013.
- Kiladis GN, von Storch H, van Loon H. 1989. Origin of the South Pacific Convergence Zone. *J. Climate* **2**: 1185–1195.
- Kummerow C, Simpson J, Thiele O, Barnes W, Chang ATC, Stocker E, Adler RF, Hou A, Kakar R, Wentz F, Ashcroft P, Kozu T, Hong Y, Okamoto K, Iguchi T, Kuroiwa H, Im E, Haddad Z, Huffman G, Ferrier B, Olson WS, Zipser E, Smith EA, Wilheit TT, North G, Krishnamurti T, Nakamura K. 2000. The status of the Tropical Rainfall Measuring Mission (TRMM) after two years in orbit. *J. Appl. Meteorol.* **39**: 1965–1982.
- Liebmann B, Smith CA. 1996. Description of a complete (interpolated) OLR dataset. *Bull. Am. Meteorol. Soc.* **77**: 1275–1277.
- Lintner BR, Neelin JD. 2008. Eastern margin variability of the South Pacific convergence zone. *Geophys. Res. Lett.* **35**: L16701. DOI:10.1029/2008GL034298.
- Matthews AJ, Kiladis GN. 1999a. The tropical–extratropical interaction between high-frequency transients and the Madden–Julian Oscillation. *Mon. Weather Rev.* **127**: 661–677.
- Matthews AJ, Kiladis GN. 1999b. Interactions between ENSO, transient circulation and tropical convection over the Pacific. *J. Climate* **12**: 3062–3086.
- Matthews AJ, Kiladis GN. 2000. A model of Rossby waves linked to submonthly convection over the eastern tropical Pacific. *J. Atmos. Sci.* **57**: 3785–3798.
- Matthews AJ, Li HYY. 2005. Modulation of station rainfall over the western Pacific by the Madden–Julian Oscillation. *Geophys. Res. Lett.* **32**: L14827. DOI:10.1029/2005GL023595.
- Matthews AJ, Hoskins BJ, Slingo JM, Blackburn M. 1996. Development of convection along the SPCZ within a Madden–Julian Oscillation. *Q. J. R. Meteorol. Soc.* **122**: 669–688.
- Meehl GA, Lukas R, Kiladis GN, Weickmann KM, Matthews AJ, Wheeler M. 2001. A conceptual framework for time and space scale interactions in the climate system. *Climate Dyn.* **17**: 753–775.
- North GR, Bell TL, Cahalan RF, Moeng FJ. 1982. Sampling errors in the estimation of empirical orthogonal functions. *Mon. Weather Rev.* **110**: 699–706.
- Pohl B, Fauchereau N, Richard Y, Rouault M, Reason CJC. 2009. Interactions between synoptic, intraseasonal and interannual convective variability over Southern Africa. *Climate Dyn.* **33**: 1033–1050.
- Reynolds RW, Rayner NA, Smith TM, Stokes DC, Wang W. 2002. An improved in situ and satellite SST analysis for climate. *J. Climate* **15**: 1609–1625.
- Slingo JM. 1998. Extratropical forcing of tropical convection in a northern winter simulation with the UGAMP GCM. *Q. J. R. Meteorol. Soc.* **124**: 27–52.
- Streten NA. 1973. Some characteristics of satellite-observed bands of persistent cloudiness over the Southern Hemisphere. *Mon. Weather Rev.* **101**: 486–495.
- Takahashi K, Battisti DS. 2007. Processes controlling the mean tropical Pacific precipitation pattern. Part II: The SPCZ and the southeast Pacific dry zone. *J. Climate* **20**: 5696–5706.
- Trenberth KE. 1976. Spatial and temporal variations of the Southern Oscillation. *Q. J. R. Meteorol. Soc.* **102**: 639–653.
- Vincent DG. 1994. The South Pacific convergence zone (SPCZ): A review. *Mon. Weather Rev.* **122**: 1949–1970.
- Vincent EM, Lengaigne M, Menkes CE, Jourdain NC, Marchesio P, Madec G. 2011. Interannual variability of the South Pacific Convergence Zone and implications for tropical cyclone genesis. *Climate Dyn.* **36**: 1881–1896.
- Webster PJ, Chang HR. 1998. Atmospheric wave propagation in heterogeneous flow: basic controls on tropical–extratropical interaction and equatorial wave modification. *Dyn. Atmos. Oceans* **27**: 91–134.
- Webster PJ, Holton JR. 1982. Cross-equatorial response to middle-latitude forcing in a zonally varying basic state. *J. Atmos. Sci.* **39**: 722–733.
- Wheeler M, Hendon HH. 2004. An all-season real-time multivariate MJO Index: Development of an index for monitoring and precipitation. *Mon. Weather Rev.* **132**: 1917–1932.
- Wheeler M, Kiladis GN. 1999. Convectively coupled equatorial waves: Analysis of clouds and temperature in the wavenumber–frequency domain. *J. Atmos. Sci.* **56**: 374–399.
- Widlansky MJ, Webster PJ, Hoyos CD. 2011. On the location and orientation of the South Pacific Convergence Zone. *Climate Dyn.* **36**: 561–578.
- Wilks DS. 2005. *Statistical methods in the atmospheric sciences*.
- Yang G-Y, Hoskins BJ. 1996. Propagation of Rossby waves of nonzero frequency. *J. Atmos. Sci.* **53**: 2365–2378.